Supporting Information

Unraveling the mechanism of the one-pot synthesis of exchange coupled Co-based nano-heterostructures with high energy product

Beatrice Muzzi,[a, b, c] Martin Albino,[c] Claudia Innocenti, [b, c] Michele Petrecca, [b, c,]* Brunetto Cortigiani,[c] César de Julián Fernández,[d] Giovanni Bertoni,[d, e] Rodrigo Fernandez-Pacheco,[g, h, i] Alfonso Ibarra,[g, h, i] Clara Marquina, [f, g] M. Ricardo Ibarra, [f, g, h, i] Claudio Sangregorio [b, c, *]

a Dept. of Biotechnology, Chemistry and Pharmacy, University of Siena 1240, I-53100 Siena, Italy

b ICCOM - CNR, I-50019 Sesto Fiorentino (FI), Italy

c Dept. of Chemistry "U. Schiff", University of Florence and INSTM, I-50019 Sesto Fiorentino (FI), Italy

d IMEM - CNR, I-43124 Parma, Italy

e CNR – Istituto Nanoscienze, I-41125 Modena, Italy

f Instituto de Ciencia de Materiales de Aragón (ICMA), Consejo Superior de Investigaciones Científicas (CSIC)-Universidad de Zaragoza, 50009-Zaragoza, Spain

g Dpto. de Física de la Materia Condensada, Universidad de Zaragoza, 50009-Zaragoza, Spain

h Instituto de Nanociencia de Aragón (INA), Universidad de Zaragoza, 50018-Zaragoza, Spain

i Laboratorio de Microscopias Avanzadas (LMA), Universidad de Zaragoza, 50018- Zaragoza, Spain

S1. Transmission electron microscopy characterization (TEM)

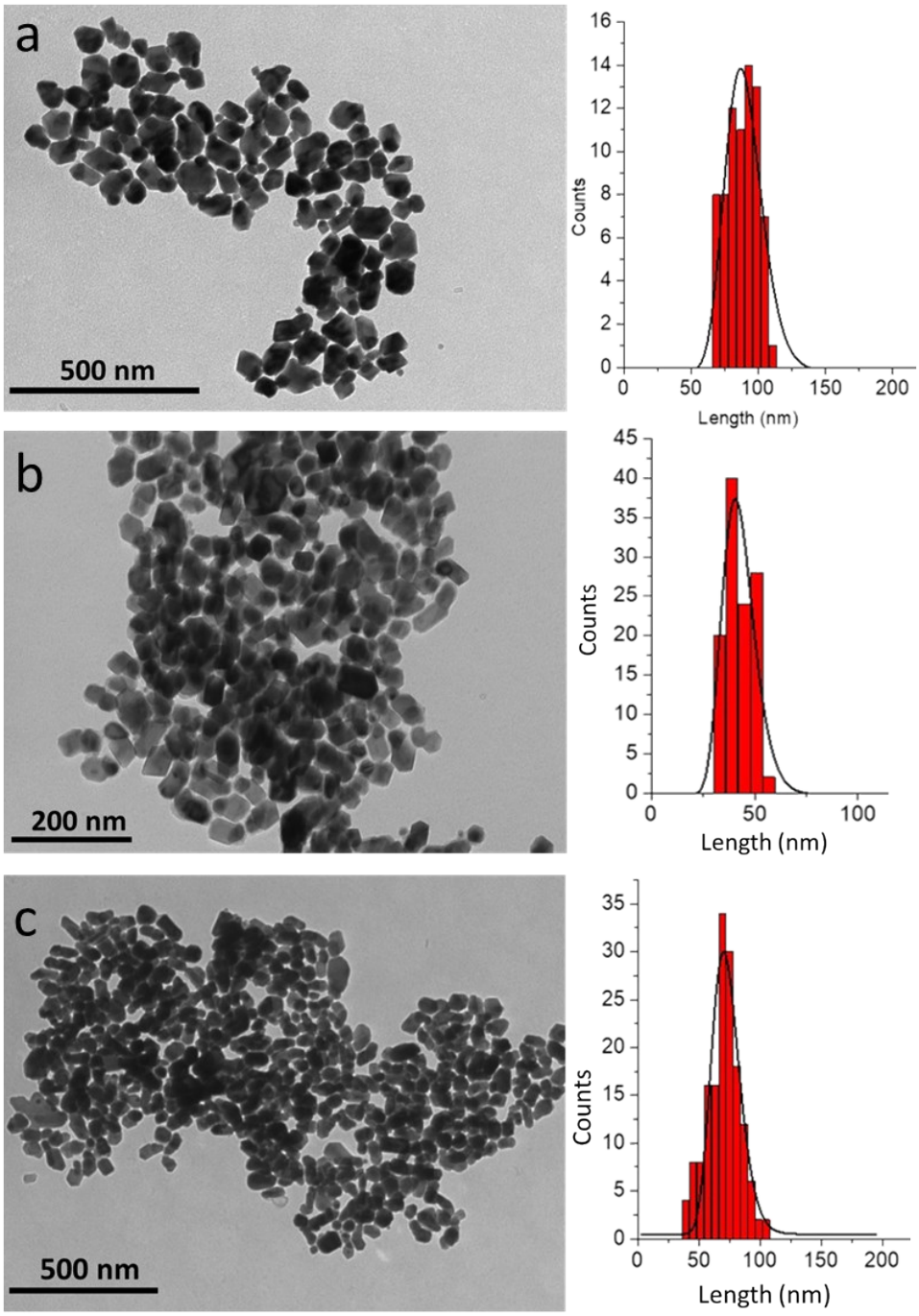

Fig. S1 Representative TEM bright field images of *a*) NHS-1, *b*) NHS-2 and *c*) NHS-3 NPs, and the corresponding size distributions. The samples consist of polydisperse and polyhedral NPs with an average diameter of ca. 90 ± 12 nm, 40 ± 6 nm and 70 ± 10 nm, respectively, as evaluated considering the length along the elongation axis.

S2. XPS characterization

XPS spectra were acquired on powder pressed on a KBr pellet, and then applying a series of sputtering and spectrum acquisition cycles (removing ca. 5 nm thickness per cycle) until a constant spectrum profile was obtained. Each sputtering process was carried out for 30 minutes. Here we report the evolution of XPS spectra after each cycle, until a constant spectrum was reached.

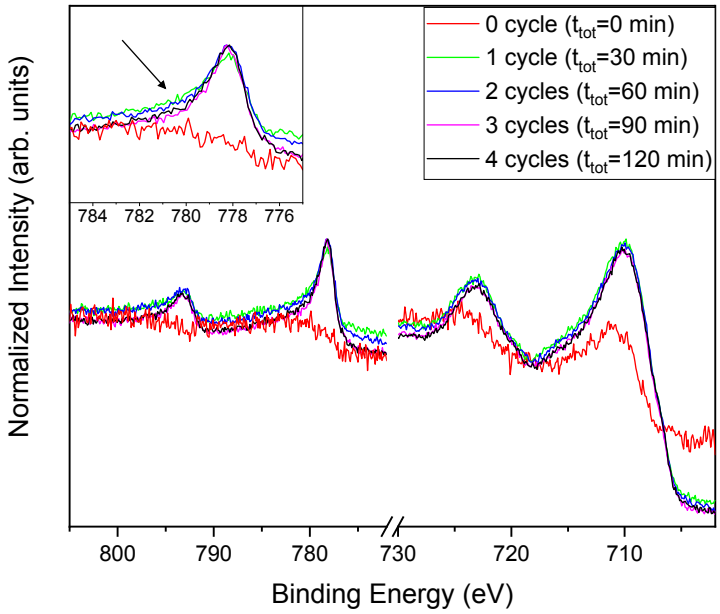

Fig. S2 XPS spectra of the iron (730 - 703 eV) and cobalt (805 – 776 eV) regions as a function of the sputtering time for sample NHS-1. The inset shows the Co $2p_{3/2}$ peak and displays the reduction of the full width at half maximum (FWHM) of the peaks on repeating the sputtering cycles; at the same time the component of metal cobalt increases, while the intensity of the shoulder at higher binding energy, related to the oxidized species, reduces.

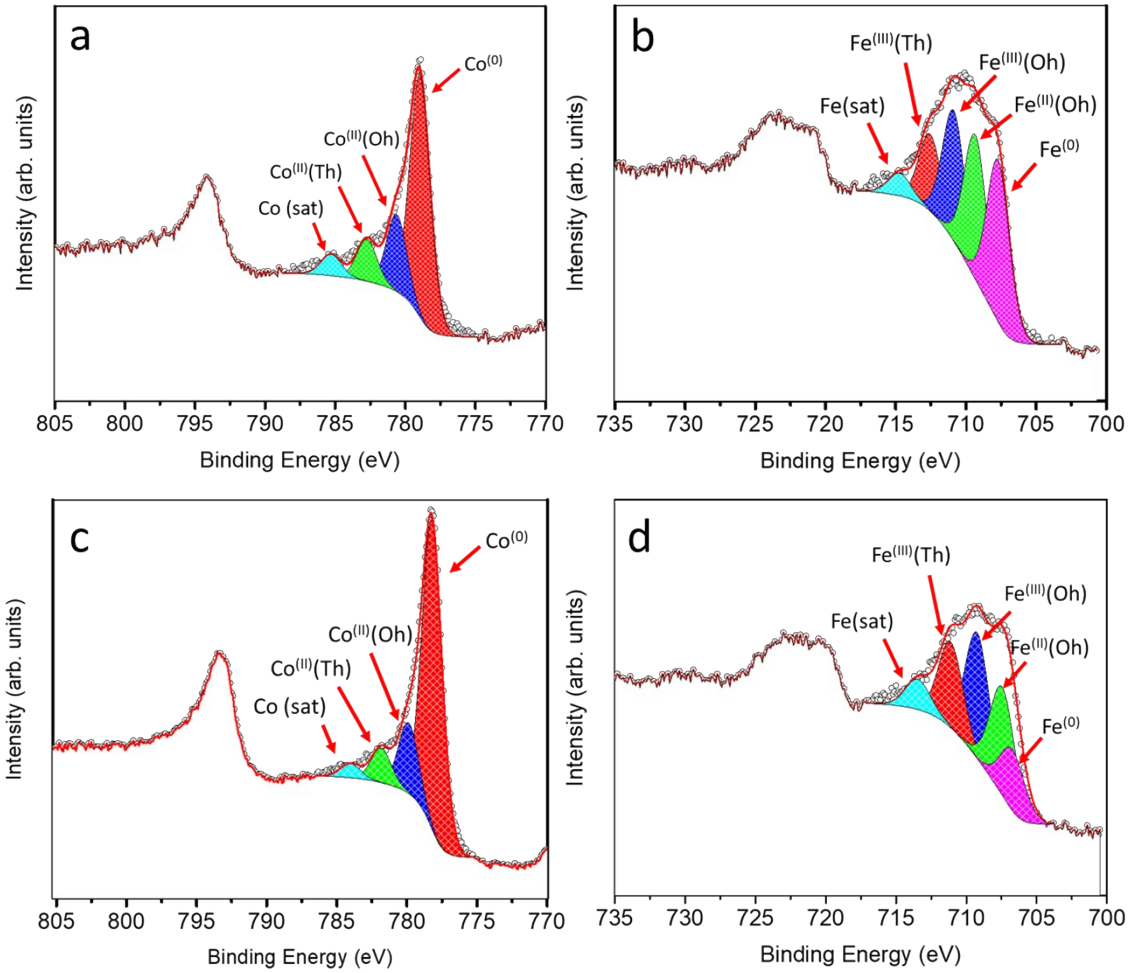

Fig. S3 XPS spectra of NHS-2 (*a, b*) and NHS-3 (*c, d*) in the region of cobalt (left) and iron (right). Spectra were recorded after four ion beam etching cycles (removing ca. 5 nm thickness per cycle). The Co $2p_{3/2}$ peak was fitted with four components: $Co^{(0)}$ metal (red peak at 778.2 eV), $Co^{(II)}$ in octahedral (*Oh*) and tetrahedral (*Td*) sites of the $Co_yFe_{3-y}O_4$ (blue and green peaks at 780 and 782.4 eV, respectively) and, a satellite peak at 784.7 eV . The Fe $2p_{3/2}$ peak was deconvoluted by five components: $Fe^{(0)}$ metal at 706.7 eV (purple peak), the three components at 708.9 eV (green), 710.7 eV (blue) and 712.7 eV (red) were ascribed to octahedral $Fe^{(II)}$ / $Fe^{(III)}$ and tetrahedral $Fe^{(III)}$, respectively, and a satellite peak at 715.3 eV.

S3. EELS elemental quantification and mapping

The spectrum images (x, y, E) were fitted at each (x, y) pixel using a model based technique[1] and Maximum Likelihood goodness of fit,[2] which is demonstrated to give the best precision and accuracy for Poisson noise, and permits to estimate the precision (as the variance of the parameters estimates) from the Cramér–Rao lower bound (CRLB), by knowing the noise level.[3] We used a simple model consisting of a power-law background, and three Hartree-Slater atomic models (σ_1, σ_2, σ_3) for the O-K, Fe-$L_{2,3}$, and Co-$L_{2,3}$ ionization edges, respectively. To account for the detailed fine structures of the edges, we have used three equalization functions (f_1, f_2, f_3) of equally distributed points (10 points for O-K edge, and 15 points for Fe-$L_{2,3}$ and Co-$L_{2,3}$, respectively):

$$f(x,y,E)=A(x,y)E^{-r(x,y)} + c_1(x,y)f_1(E)\sigma_1(\alpha,\beta,E) + c_2(x,y)f_2(E)\sigma_2(\alpha,\beta,E) + c_3(x,y)f_3(E)\sigma_3(\alpha,\beta,E) \quad \text{eq.S1}$$

Due to the small thickness of the particles we neglected the effects of multiple scattering through the sample. The resulting fitting model for the integrated area 1 of Figure 4c, main text (oxide shell of the particle) is presented in Figure S2a, demonstrating the overall good quality of the fit. The Co/Fe ratio calculated is 1.01(6), which corresponds to an equal amount of Co and Fe in the oxide. The estimated parameters c_1, c_2, c_3 are presented in Figure S2b, which gives the distribution in the selected area for O, Fe, and Co, respectively.

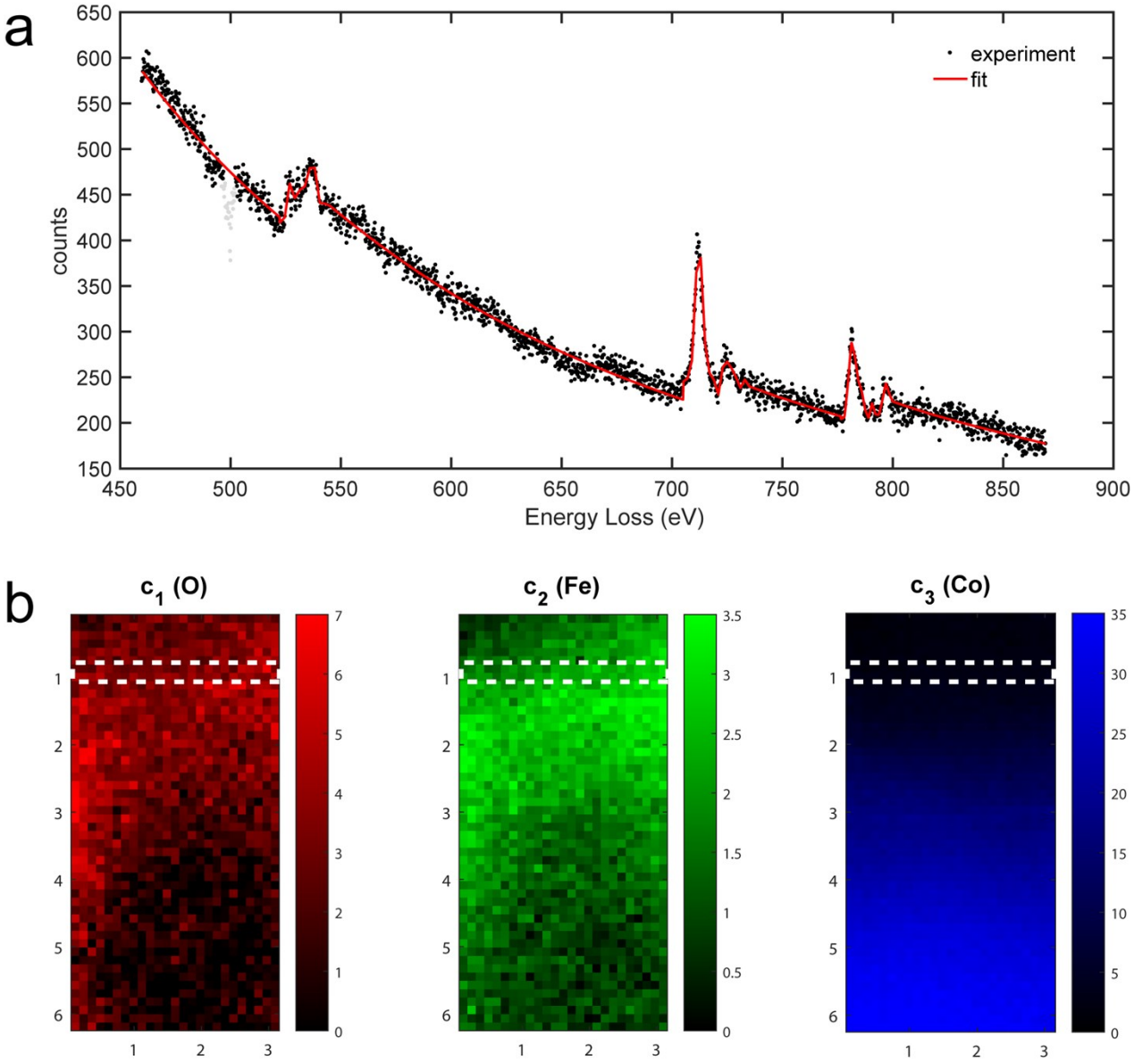

Fig. S4 a) Experimental spectrum (black dots) and resulting fit (full red line) according to eq.1 as obtained from the integrated area 1 of Figure 4c of the manuscript (sample NHS-1). Some points (light gray) preceding the O-K edge were excluded, as they derived from the temporary common saturation of the CCD with the elastic peak during the tuning of the spectrometer. b) Estimated parameters c_1, c_2, c_3 from eq.1, which gives the O, Fe, and Co elemental maps, respectively.

S4. Magnetic characterization

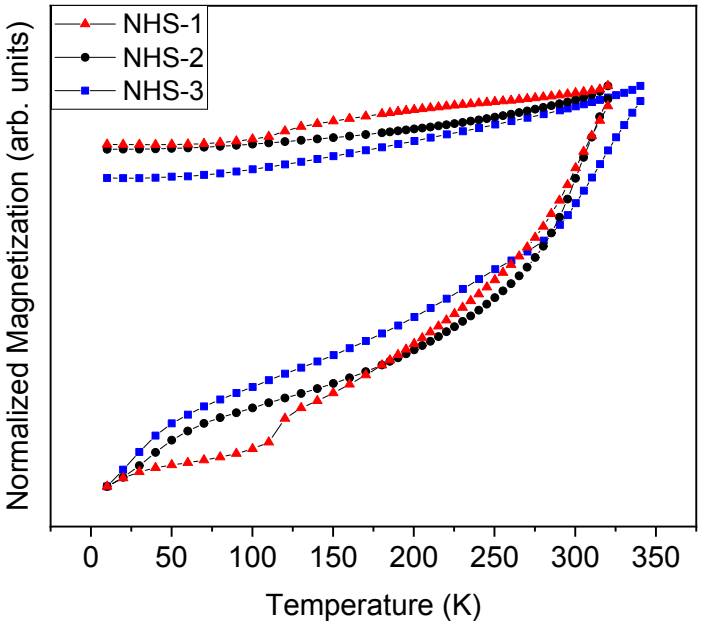

Fig. S5 Temperature dependence of the magnetization recorded after ZFC and FC processes for NHS-1, NHS-2 and NHS-3 applying a constant magnetic field of 5 mT.

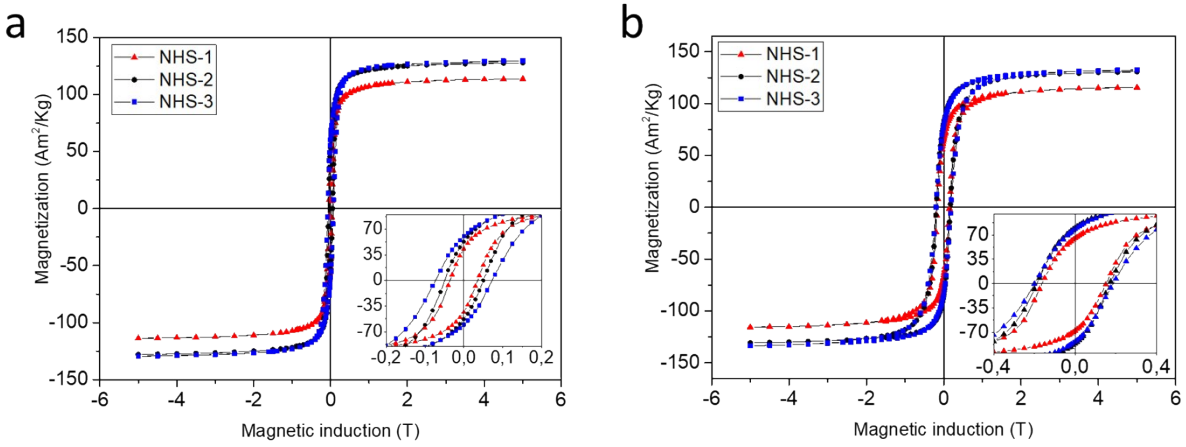

Fig. S6 Hysteresis loops recorded at room temperature (*a*) and at 5 K (*b*) for NHS-1, NHS-2 and NHS-3 samples; the insets show the magnification of the low field region.

S5. The fundamental role of NaOL as reducing agent.

Four syntheses using a variable weight ratio of OA to NaOL, while keeping the precursor to surfactants ratio constant (ca. 0.6), were performed. The syntheses were carried out dissolving the precursor and the surfactants in 10 mL of docosane at 80 °C. The mixture was heated from 80 to 370 °C, at 2.9 °C min^{-1}, under vigorous stirring and nitrogen flux. The suspension was kept at 370 °C for 40 minutes and let cooling to room temperature. The resulting black powder was separated by application of an external magnet, washed with 2-propanol, hexane and ethanol and finally dried under nitrogen flux. Precursor and surfactants used for the four syntheses are reported in Table S1.

Table S1 *Amount of precursor and surfactants used for the four syntheses.*

Sample Name	**1-FeCoOL**	**Oleic Acid (OA)**	**Sodium Oleate (NaOL)**
1-FeCoOL + 100 % OA	1.50 g (ca. 2 mmol)	1.00 g (3.5 mmol)	-
1-FeCoOL + 90 % of OA + 10 % NaOL	1.50 g (ca. 2 mmol)	0.90 g (3.2 mmol)	0.10 g (0.3 mmol)
1-FeCoOL + 50 % of OA + 50 % NaOL	1.50 g (ca. 2 mmol)	0.57 g (2 mmol)	0.57 g (1.8 mmol)
1-FeCoOL + 100 % NaOL	1.50 g (ca. 2 mmol)	-	1.06 g (3.5 mmol)

S6. XRD characterization

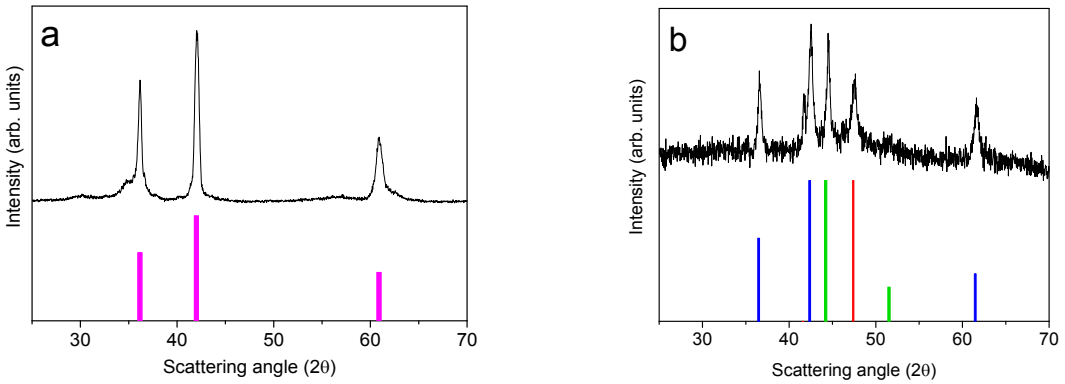

Fig. S7 XRD patterns of nanopowders obtained by thermal decomposition of FeOL (*a*) and CoOL (*b*), using an oleic acid and sodium oleate 1:1 mixture. Reference bars: FeO (*JCPDS PDF #74-1884)*; CoO (*JCPDS PDF #71-1178*); *hcp* $Co^{(0)}$ (*JCPDS PDF #89-7373*) and *fcc* $Co^{(0)}$, (*JCPDS PDF #15-0806*).

S7. Investigation on long-term stability under air exposure

XRD characterization

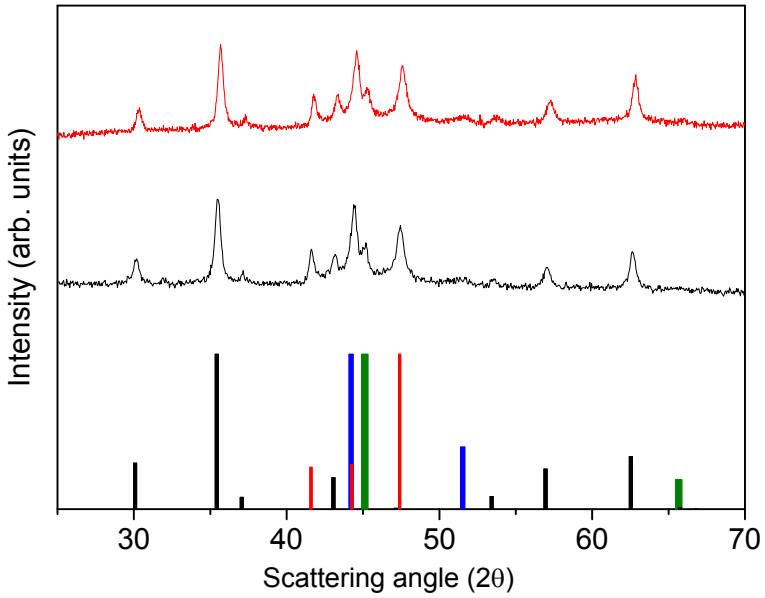

Fig. S8 Experimental XRD patterns of NHS-3 as prepared (black line) and after exposure to air for one year (red line) with reference patterns of: $CoFe_2O_4$, (*JCPDS PDF #22-1086*); *hcp* $Co^{(0)}$ (*JCPDS PDF #89-7373*); *fcc* $Co^{(0)}$, (*JCPDS PDF #15-0806*), and Co-Fe alloy, (*JCPDS PDF #65-4131*). Rietveld refinement of the two patterns did not show any relevant variation in the lattice parameters, average crystallite sizes and phase percentages (Table S2).

Table S2: *Saturation magnetization, remanence and coercive field obtained from hysteresis loops recorded at 5 K on the as prepared NHS-3 and after exposure to air for one year. Phase percentage (w/w) obtained from Rietveld refinement of XRD patterns of NHS-3 as prepared and after one year.*

	Magnetic Properties						**XRD Phase percentage % (w/w)**		
	As prepared			After one year			Crystal phase	As prepared	After one year
NHS-3	M_S	M_r	μ_0H_C	M_S	M_r	μ_0H_C	Co (fcc)	21 (2)	19 (2)
	(emu/g)		(T)	(emu/g)		(T)	Co (hcp)	12 (2)	13 (2)
	133	79	0.02	130	79	0.02	Co-Fe Alloy	9 (3)	10 (3)
							$Co_yFe_{3-y}O_4$	57 (2)	58 (2)

Magnetic properties

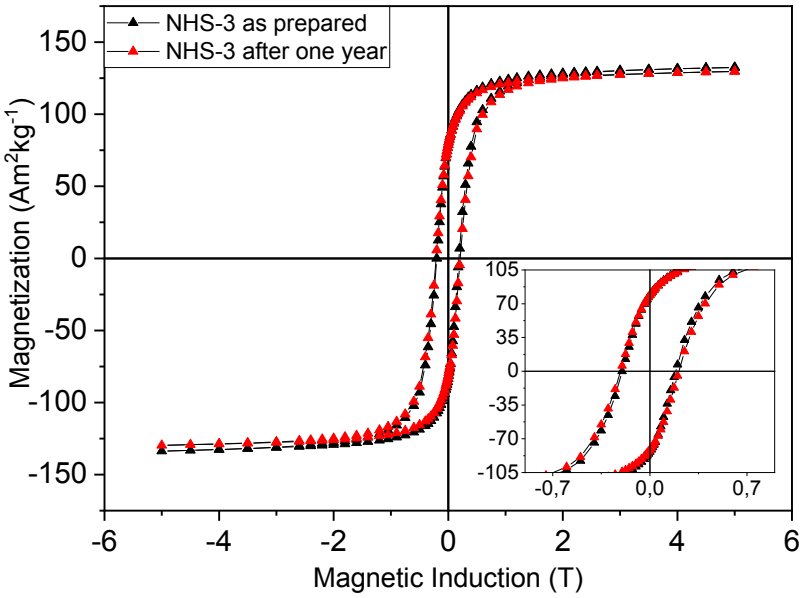

Fig. S9 Hysteresis loops recorded at 5 K of NHS-3 as prepared (black line) and after exposure to air for one year (red line); the inset shows the magnification of the low field region.

S8. Thermal gravimetric analysis (TGA)

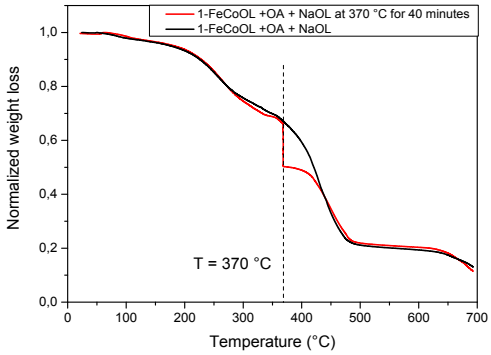

Fig. S10 TGA curves of 1-FeCoOL in the presence of OA and NaOL measured with a standard temperature ramp (black line) and adding an isothermal dwell of 40 minutes at 370 °C (red line). The black curve shows, after a small humidity loss below 100 °C, two steps: a first one at ca. 260 °C (ca. 25 %) and a more pronounced (ca. 50 %), second one at ca. 430 °C, for a total weight loss of ca. 75 %. The red curve shows the profile of the same mixture measured under the same conditions but adding an isothermal dwell of 40 minutes at 370 °C, which corresponds to the conditions used in the thermal decomposition synthesis of the NHSs. The comparison of the two curves proves that, at the selected chosen reaction time, the decomposition of the metal precursor occurs without the complete degradation of the surfactants.

S9. Morphology and magnetic properties of samples obtained after 10 and 25 minutes of reaction time.

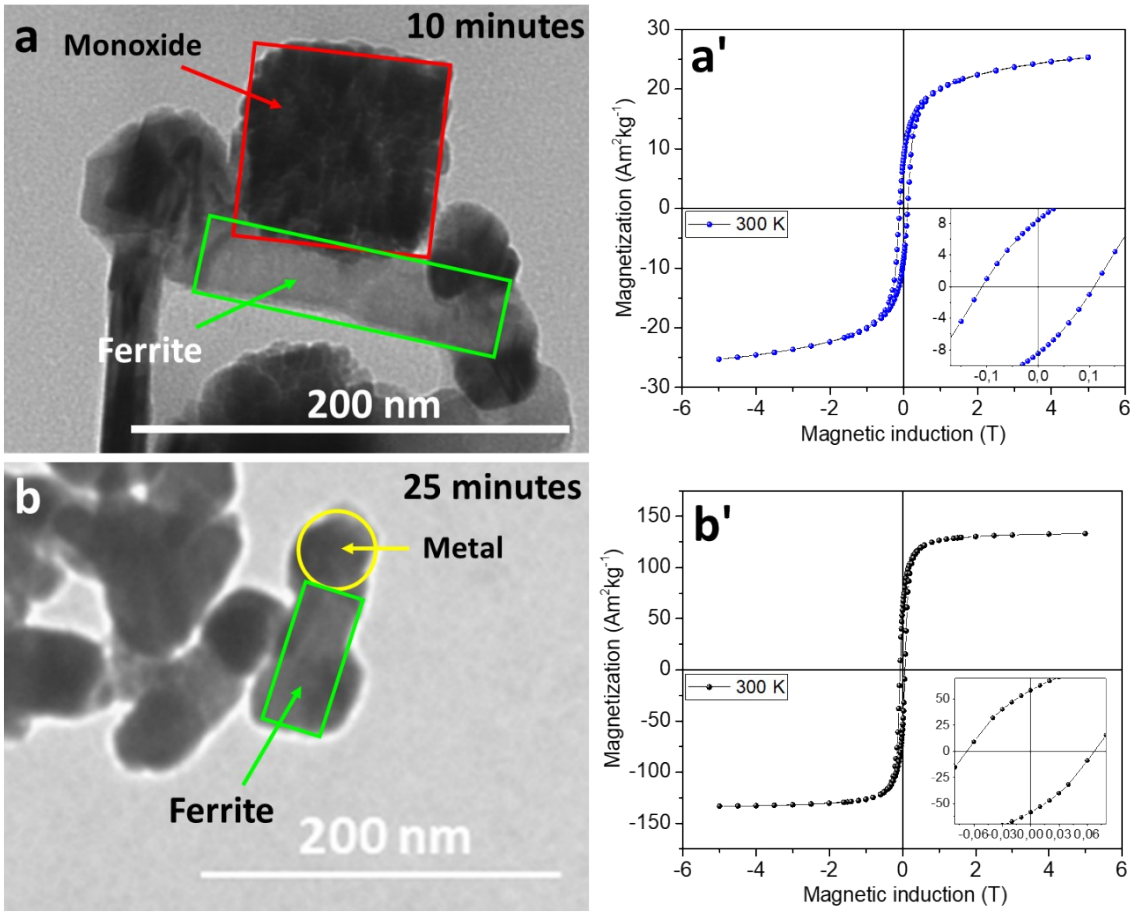

Fig. S11 Left: TEM images of the samples obtained after 10 (*a*) and 25 minutes (*b*) of reaction time. Red, green and yellow boxes identify monoxide ($Co_{1-x}Fe_xO$), ferrite ($Co_yFe_{1-y}Fe_2O_4$) and metal phases (*fcc* $Co^{(0)}$), respectively. Right: Hysteresis loops recorded at 300 K of the samples obtained after 10 (*a'*) and 25 minutes (*b'*).

References

1 G. Bertoni and J. Verbeeck, *Ultramicroscopy*, 2008, **108**, 782–790.

2 J. Verbeeck and S. Van Aert, *Ultramicroscopy*, 2004, **101**, 207–224.

3 J. Verbeeck and G. Bertoni, *Ultramicroscopy*, 2008, **108**, 74–83.